BASIC SCIENCE

Nanomedicine: Nanotechnology, Biology, and Medicine
9 (2013) 1328–1335

Research Article

nanomedjournal.com

In-vitro cyto-toxicity, geno-toxicity, and bio-imaging evaluation of one-pot synthesized luminescent functionalized mesoporous SiO_2@$Eu(OH)_3$ core-shell microspheres

Anees A. Ansari, PhD[a,*], Tarique N. Hasan, PhD[b], Naveed A. Syed, MSc[b], Joselito P. Labis, PhD[a], A.K. Parchur, PhD[c], Gowhar Shafi, PhD[d], Ali A. Alshatwi, PhD[b]

[a]*King Abdullah Institute for Nanotechnology, King Saud University, Riyadh, Saudi Arabia*
[b]*Molecular Cancer Biology Research Lab (MCBRL), Department of Food Science and Nutrition, King Saud University, Riyadh, Saudi Arabia*
[c]*Department of Physics, Banaras Hindu University, Varanasi, India*
[d]*Department of Molecular Biology, Institute of Genetics and Hospital for Genetic Diseases Hyderabad, India*

Received 20 February 2013; accepted 13 May 2013

Abstract

Luminescent functionalized mesoporous SiO_2@$Eu(OH)_3$ core-shell microspheres (LFMCSMs) were prepared by coating of europium hydroxide ($Eu(OH)_3$) shell on mesoporous silica (SiO_2) nanospheres via a facile one-pot process at low temperature. The FETEM images revealed that a well-defined luminescent europium hydroxide shell was successfully grafted on the surface of mesoporous silica nanospheres. These experimental results showed that the LFMCSM has a typical diameter of ca. 392 nm consisting of the silica core with about 230 nm in diameter and europium hydroxide shell with an average thickness of about 162 nm. LFMCSMs exhibited strong red emission peak upon irradiation with ultraviolet light, which originated from the electric-dipole transition $^5D_0 \rightarrow {}^7F_2$ (614 nm) of Eu^{3+} ion. The biocompatibility of the synthesized LFMCSMs was evaluated in vitro by assessing their cytotoxic and genotoxic effect on human hepatoblastoma (HepG2) cells using MTT, TUNEL, fluorescent staining, DNA ladder and Gene expression assays respectively.

From the Clinical Editor: This paper describes the development of a one-pot synthesis of luminescent mesoporous SiO_2@$Eu(OH)_3$ core-shell microspheres and evaluates their favorable *in vitro* cyto-toxicity and geno-toxicity, and their applications in bio-imaging of these particles that emit bright red signal under UV exposure.

Key words: Luminescent functionalized mesoporous SiO_2@$Eu(OH)_3$ core-shell microspheres; Photoluminescence; Genotoxicity and cytotoxicity

In recent years, luminescent mesoporous nanomaterials (LMNs) have become an attractive research field because of their great potential in biological applications such as MRI contrast agent, drug-delivery carrier, biomarkers, diagnostic analysis and as well as fluorescent proteins biolabeling.[1–3] A key challenge in these applications is the synthesis of LMNs with controlled size, composition, and surface properties, which has been the subject of research of an increasingly interdisciplinary nature. In many areas of biological application, the ability to engineer surface properties is important because LMNs are desired to have the required biocompatibility and interfacial reactivity.[4–6] Significant progress has been made for bottom-up fabrication of LMNs including luminescent semiconductor nanoparticles (quantum dots),[7] plasmon-resonant nanoparticles,[8] gold nanoparticles[9] and luminophore-doped silica nanoparticles,[10] via chemical processes such as decomposition, reduction, or oxidation reactions in both aqueous and organic media. It is known that some luminescent nanoparticles, such as quantum dots and luminophore-doped silica nanoparticles have been used as luminescence probes as they have stronger luminescence and higher photo-stability compared with conventional organic dyes.[7,11] The main problem in the applications of the LMNs as a luminescence probes is that the luminescence measurement is easily affected by strong non-specific scattering light, such as Tyndall, Rayleigh and Raman scatterings.[9–11] This problem has limited their effective application for quantitative bioassays. In fact, the uses of the LMNs as a luminescence probes

Conflict of interest: All authors in this manuscript do not have any conflict of interest.

Funding: No funding.

*Corresponding author. King Abdullah Institute for Nanotechnology, King Saud University, Riyadh, Saudi Arabia.

E-mail address: aneesaansari@gmail.com (A.A. Ansari).

1549-9634/$ – see front matter.
http://dx.doi.org/10.1016/j.nano.2013.05.006

Please cite this article as: Ansari AA, et al, *In-vitro* cyto-toxicity, geno-toxicity and bio-imaging evaluation of one-pot synthesized luminescent functionalized mesoporous SiO_2@$Eu(OH)_3$ core-shell. *Nanomedicine: NBM* 2013;9:1328-1335, http://dx.doi.org/10.1016/j.nano.2013.05.006

in bioassays are mainly qualitative or semi-quantitative. In order to address these key issues, it is important to develop a shell of an alternate luminescent material to control these parameters. Among many approaches to the modification or functionalization of the surfaces of LMNs with materials such as polymeric materials, organic monolayers and metals, one of the most promising systems involve silica microspheres coated with luminescent shells. This type of core-shell nanoparticle, e.g., silica@$Ln(OH)_3$, not only provides enhanced stabilization, but also allows fine-tuning of the surface biocompatibility and luminescence properties such as sharp absorption and emission lines, high quantum yields, long lifetimes and superior photo-stability.[8]

In this study, we present a simple, but efficient wet chemical route for constructing a luminescent functionalized mesoporous SiO_2@$Eu(OH)_3$ core-shell microspheres with tunable dimensions (200-240 nm in diameter), in which each nanosphere is composed of silica nanosphere as the core and an outer thick shell of europium hydroxide was successfully covered (designated as SiO_2@$Eu(OH)_3$). In addition, an initial assessment of the biocompatibility of these microspheres was performed using an MTT cell viability assay. To the best of our knowledge, this is the first report of the successful coating of the micro-size, uniformity, and monodispersity of luminescent functionalized mesoporous SiO_2@$Eu(OH)_3$ core-shell microspheres.

Methods

Materials and methods

Europium oxide (99.99%, Alfa Aesar, Germany), Tetraethyl orthosilicate (TEOS, 99 wt% analytical reagent A.R.), C_2H_5OH, HNO_3 and NH_4OH were used as starting materials without any further purification. $Eu(NO_3)_36H_2O$ were prepared by dissolving the corresponding oxide in diluted nitric acid, and nanopure water was used for preparation of solutions. Ultrapure de-ionized water was prepared using a Milli-Q system (Millipore, Bedford, MA, USA). All other chemicals used were of reagent grade (*more information about synthesis and results discussion in supplementary materials*).

Results

Synthesis, structural measurement and morphology of the LFMCSM

Figure 1, *A* shows the wide angle X-Ray diffraction pattern (XRD) of LFMCSM. Sample shows a broad peak around ~2θ = 22° is because of amorphous phase of SiO_2 nanospheres and no sharp diffraction peak corresponding to crystalline structure is observed. There are no detectable diffractions of the Eu^{3+} ions in crystalline phase observed due to the existence of amorphous silica and europium hydroxide components or ultra-small crystalline materials where diffraction peaks cannot be well resolved. Therefore, it could be due to the luminescent functionalized (Eu^{3+}) in the silica framework expanded the nanopores and rearranged the Si-O-Si and -Si-O-Eu-O-H-network structures without any impurities. Similar results are reported in the literature on mesoporous silica functionalized with luminescent materials and silica coated iron oxide nanoparticles.[4,5,12] In our case europium hydroxide molecules in the microspheres are in a non-crystalline or ultra small crystalline state.

The morphological and structural feature of the resulting sample was also examined by TEM. The representative FETEM micrographs of the microspheres are illustrated in Figure 1, *B* low-magnification core-shell microspheres, high-magnification single LFMCSM part (Figure 1, *C*)) and high magnification micrograph of the outer layer (Figure 1, *D*). It is clear that the particles are almost spherical in shape having an average diameter around ~392-400 nm and non-agglomerated with mono dispersion. On our clear observation it is found that core thickness slightly varies by ~50 nm, however the shell thickness are almost constant over all particles. The FETEM micrographs clearly resolve the thickness of core and shell of each core-shell particle. Typically, the size of core is ~230 nm (in diameter) and shell is ~162 nm (thickness) (Figure 1, *D*). In the deposition of europium hydroxide layer on the surface of microspheres the morphologies of their parent microspheres are still maintained. As a result, a thick shell of europium hydroxide was successfully grafted onto the surface of silica microspheres to form SiO_2@$Eu(OH)_3$ core-shell microspheres, which would increase the polydispersity of the particles after core-shell formation. Additionally, from the TEM micrographs of LFMCSM, the core-shell structure can be clearly distinguished due to the different electron penetrability between the cores and shells (i.e., refractive index of core and shell is different). The mesoporous silica core is grey color (~230 nm, in diameter), and dark black shell europium hydroxide shell with an average thickness of about ~162 nm (Figure 1, *D*). Every core-shell microsphere has a core, confirming that the CTAB molecules served as a seed for the shell growth of SiO_2. Furthermore, no irregular particles related with the introduced phosphors were detected. The results suggest that the deposition has immense influence on the spherical morphology and the luminescent material layer uniformly grafted on the silica nanospheres surface. The thickness of the europium hydroxide shell can be tuned by simply varying the initial amount of europium nitrate. As the shell grew thicker, the core-shell spheres became more uniform and poly-dispersity improved after varying the parameters such as temperature, concentration of the base and solvent. Such LFMCSMs can be well dispersed in an aqueous medium, non-aqueous solutions (ethanol) and nonpolar (cyclohexane) organic solvent, and possess good luminescent response.

To explore the possibilities of photoluminescence properties of the microspheres, we carried out PL measurements at ambient temperature under the excitation of 325 nm (3.82 eV). The emission peaks for Eu^{3+}-based materials arise from electronic and magnetic transitions of 4*f*-4*f* electrons by direct excitation from the europium ground state into the higher excited states of the europium *f*-electrons. These 4*f* transitions are very sensitive to the location of Eu^{3+} ions within the crystal lattice, their surrounding crystal field and lattice deformations. Figure 1, *E* shows the emission spectrum of the LFMCSM under 325 nm laser excitation. The spectrum shows the typical emission peaks

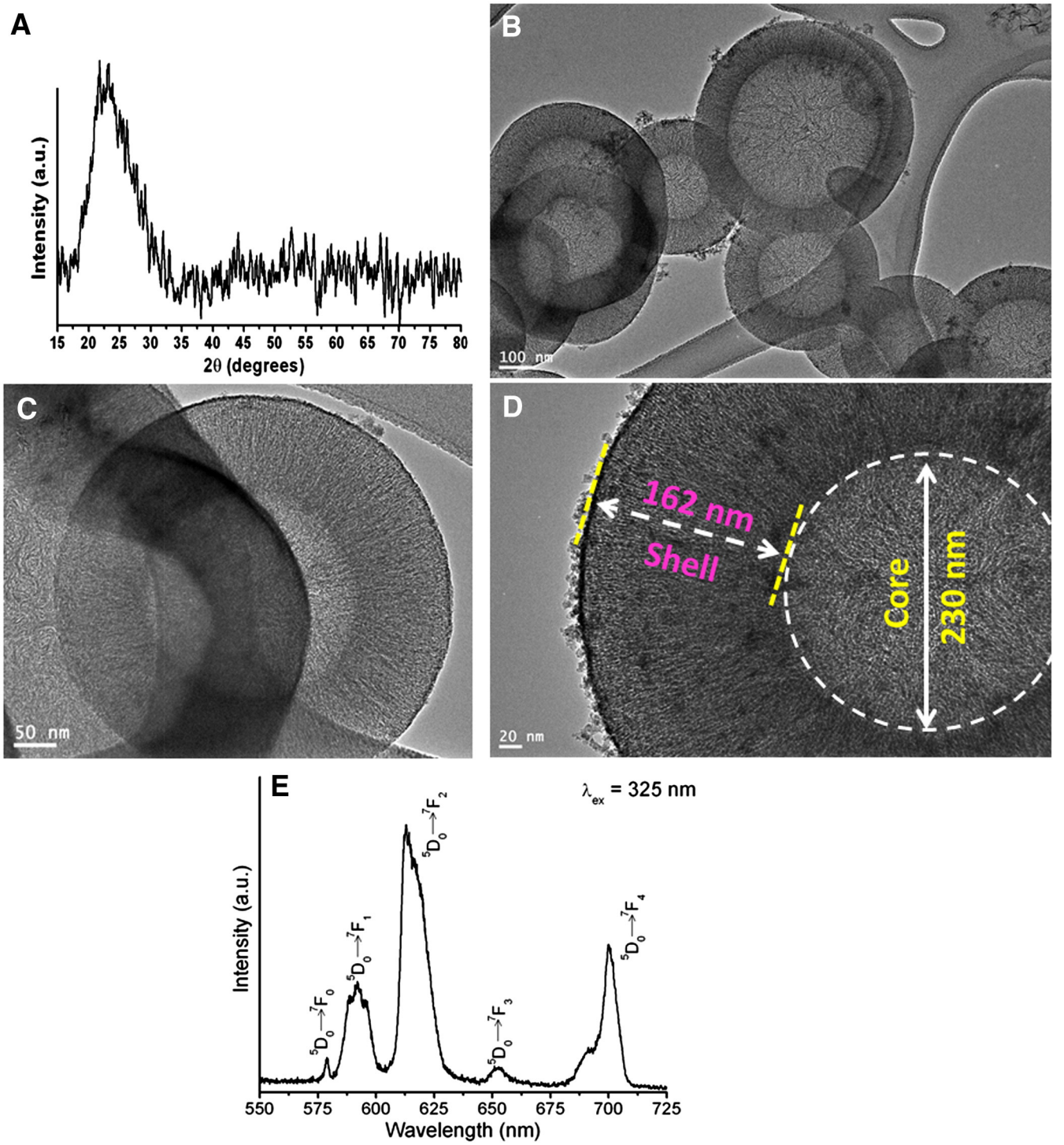

Figure 1. (**A**). Wide-angle X-ray diffraction pattern, (**B**) FE-TEM micrographs of luminescent functionalized mesoporous SiO_2@$Eu(OH)_3$ core-shell microspheres (**C**) low-magnification micrographs of the outer layer, (**D**) single luminescent functionalized mesoporous SiO_2@$Eu(OH)_3$ core-shell microspheres, (**E**). Photoluminescence spectrum of luminescent functionalized mesoporous SiO_2@$Eu(OH)_3$ core-shell microspheres under 325 nm excitation.

of Eu^{3+} ions at ~577 (2.14), 591 (2.09), 614 (2.02), 652 (1.9), and 700 nm (1.77 eV) and can be attributed to transitions from the $^5D_0$ level to sublevel of $^7F_0$, $^7F_1$, $^7F_2$, $^7F_3$, and $^7F_4$, respectively.[13–15] The strong prominent electric dipole transition ($^5D_0 \rightarrow {}^7F_2$) located at 614 nm, corresponding to the red emission and the magnetic dipole transition ($^5D_0 \rightarrow {}^7F_1$) located at 591 nm corresponds to orange emission. On the average integrated emission intensity of $^5D_0 \rightarrow {}^7F_2$ transition is ~3.1 times higher than $^5D_0 \rightarrow {}^7F_1$ transition. Also, the ratio of integrated emission intensity of electric to magnetic dipole transition is called asymmetric ratio (A_{21}). Moreover, the $A_{21} > 1$ suggests that the Eu^{3+} ion occupies in asymmetric sites in shell

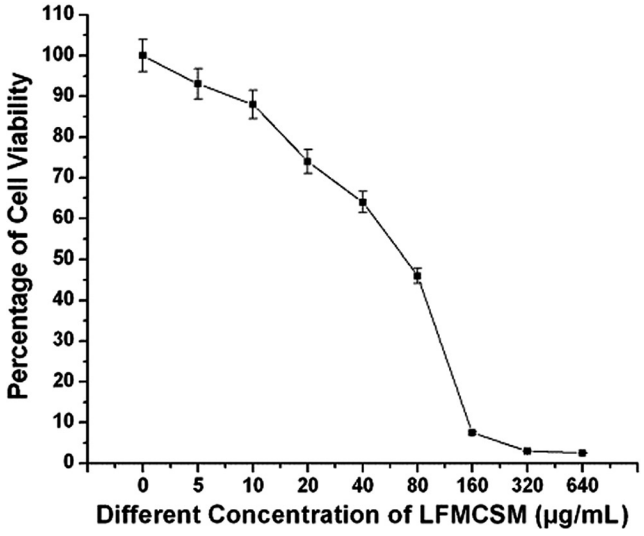

Figure 2. Evaluation of cytotoxicity by MTT assay and determination of IC_{50} of LFMCSMs against the HepG2 liver cancer cell line.

structure. Parchur et al reported A_{21} value ~10 in Eu^{3+} doped $CaMoO_4$ (i.e., Eu^{3+} ion in asymmetric environment) and ~1 in Eu^{3+} doped YPO_4 systems (i.e., Eu^{3+} ion in symmetric environment).[15] The $^5D_0 \rightarrow {}^7F_0$ transition (at 577 nm) is forbidden in accordance with Judd–Ofelt theory.[16] Smaller intensity of this transition confirms the mixing of J levels in ground state ($^7F_0$ and $^7F_1$).[15] The branching ratio (β) values are found to be ~0.2, 19.7, 60.5, 1.4 and 18.2% for $^5D_0 \rightarrow {}^7F_0$, $^5D_0 \rightarrow {}^7F_1$, $^5D_0 \rightarrow {}^7F_2$, $^5D_0 \rightarrow {}^7F_3$ and $^5D_0 \rightarrow {}^7F_4$ transitions, respectively. A more extensive investigation of the luminescent properties of the LFMCSM is required to explore their future prospects in medical sciences. In addition, the emission lines in the LFMCSM spectrum under the excitation at 325 nm are broad which are attributed to non-crystalline nature of $Eu(OH)_3$ which is supported by low angle and wide angle X-ray diffraction pattern (Figure 1, *A*). The spectrum testing results further prove the aforementioned conclusion that fluorescent $Eu(OH)_3$ molecules have be grafted on the surface of silica microspheres of the SiO_2@$Eu(OH)_3$ microspheres.

Discussion

Cytotoxicity & genotoxicity assessment and their underlying mechanism

For biomedical applications, genotoxicity, cytotoxicity and biocompatibility of the synthesized LFMCSM are the most important factors needed to be investigated. In addition, it is also necessary to minimize the particle aggregation since aggregated particles will affect not only the particle circulation inside human body, but also the particle delivery to the targeted cancer cells. As shown in Figure 2, the cytotoxicity profile of LFMCSM is determined in human hepatoblastoma HepG2 cells using an MTT assay. The LFMCSM exhibited significant cell viability at lower concentrations from 5 µg/mL to 80 µg/mL (at 24 h) as demonstrated by MTT assay. However, on increasing the LFMCSM concentrations (80, 160, 340 and 680 µg/mL) a noticeable dose-dependent decrease in their relative cell viability was observed. The decrease cell viability in the presence of high concentration of the microspheres might be due to large surface area, although a dependency of cytotoxicity on the nature of the attached functional group cannot be ruled out. It is also evident from the literature that the factors contributing to cytotoxicity may include particle size (diameter) and surface functionalization of the materials. Since cytotoxicity of LFMCSM in the applied concentration range is caused by production of hydroxyl radicals in large amount from luminescent functionalized $Eu(OH)_3$ coating.[17] It is suggested that these productive hydroxyl radicals are helpful to generate reactive oxygen species, which are responsible for cell apoptosis.[18–20] Since luminescent functionalized $Eu(OH)_3$ has surface sites similar to those found in harmful polymeric materials, it possible that the former also acts as a facilitator of reactive oxygen species through its exposed surface sites, but as outlined above, exposed surface cannot be the only factor underling cytotoxicity. However, some other options are possible for what this mechanism might be. The $Eu(OH)_3$ destabilizes the cell membrane, and may therefore allow Eu^{3+} to depolarize the cells by affecting the electron transport chain. The small amounts of Eu^{3+} and ROS released even during dark conditions might be highly effective because of their proximity to the cell. The Eu^{3+} might also make $Eu(OH)_3$ more reactive by oxidizing the peptide, which could lead to the formation of long-lived ROS such as peroxide.[21] Once a metal-containing particle has penetrated the cells, metal ions can leach from the particle and generate ROS in the cell interior leading to oxidative stress to cells—in what is called a "Trojan horse" mechanism.[22]

The different assays are performed on LFMCSM for measuring the cell apoptosis in accord with the published literature reports.[23–26] The HepG2 cells and genomic DNA are exploited for determination of cells apoptosis, this apoptosis assay is supported by DNA Ladder and TUNEL (dUTP nick-end labeling) assay, respectively, as shown in Figures 3 & 4. These two assays measure two different phenomena to show the fragmentation of genomic DNA. The DNA ladder assay was applied to analyze the fragmentation of the genomic DNA by gel electrophoresis whereas the TUNEL assay measures the time dependent broken DNA strands. The electrophoresis assay imaging revealed and confirmed the fragmentation of the genomic DNA as shown in Figure 3. AO/EtBr staining was also opted to quantify the early and late apoptotic cells. DAPI and PI staining assays were able to convey the nuclear fragmentation and other morphological changes in cells. Many experts argue that TUNEL assay is a better assay for cell apoptosis/cytotoxicity measurements in comparison with MTT, as it measures the DNA fragmentation, which is more directly related to the cells apoptosis.[25] According to Bhakta et al the plasmid DNA was well protected on the surface of the LFMCSMs as they are not degraded by DNase treatment.[27] Figure 4, *A* illustrates the TUNEL assay of HepG2 cells treated with Tris-EDTA buffer (− Ve control experiment) where we have not found any green apoptotic nuclei indicating no apoptosis. Figure 4, *B* shows the TUNEL assay of HepG2 cells treated with LFMCSM at the concentration of 80 µg/mL for 4 h at 37 °C as a positive inducer where green nuclei indicate the apoptosis of all

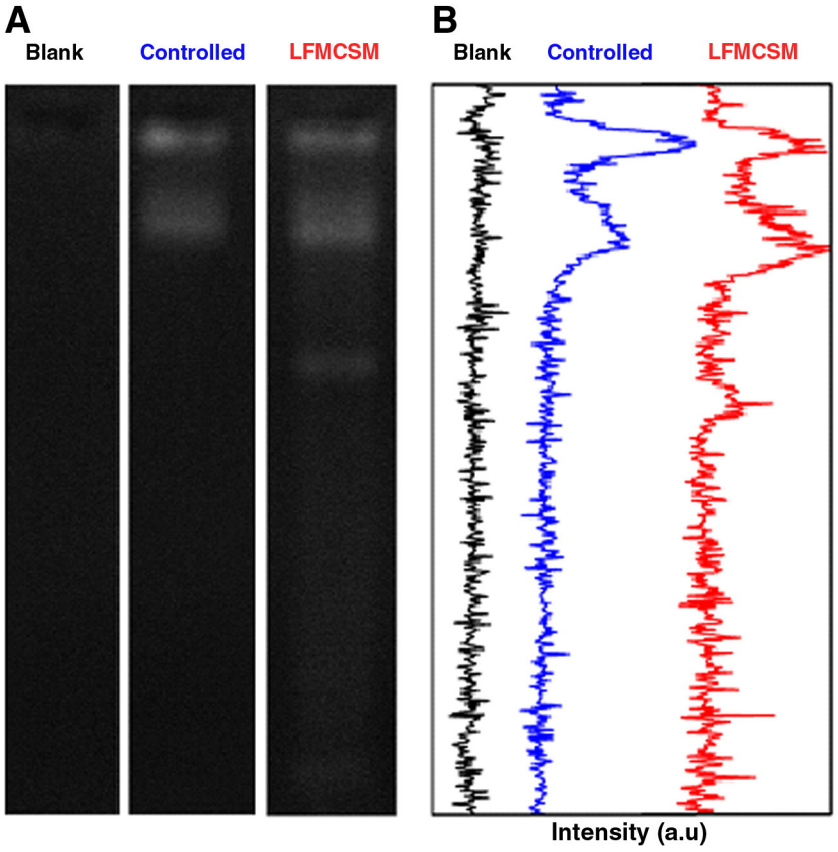

Figure 3. DNA Ladder Assay: Agarose gel electrophoresis of genomic DNA for visualization of their fragmentation as evidence of genotoxicity with respect to control (**A**), genomic DNA band intensity peaks (**B**).

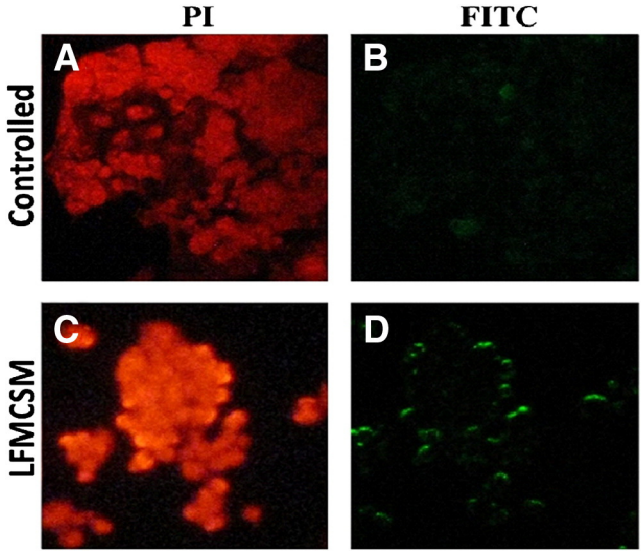

Figure 4. TUNEL assay after 24 h incubation of HepG2 cells against LFMCSMs. Red fluorescence is due to Propidium Iodide staining and observed under green filter while green fluorescence is due to FITC staining and observed under blue filter. Observations done at 400× magnification.

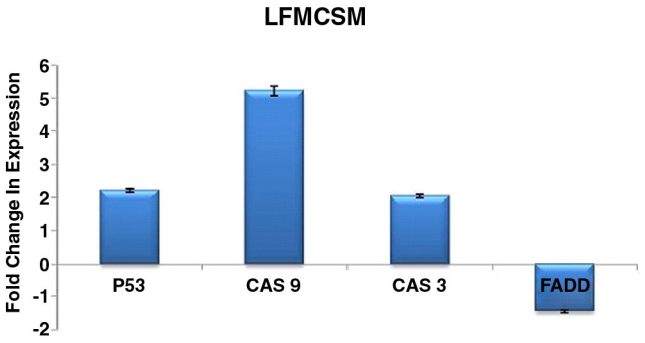

Figure 5. Comparative study of apoptosis related genes expressions as fold change (ratio of target: reference gene) in HepG2 cells after exposure of LFMCSMs up to 24 h.

genomic DNA. The hydroxyl (OH) surface group induced oxidative stress leads to DNA damage and apoptosis.[28] These results are in agreement with previous literature reports where hydroxyl group on mesoporous silica nanoparticles induced ROS mediated apoptosis in human neuroblastoma (SK–N–SH) cells.[29,30] Stone et al have suggested that surface reactivity plays an important role in ROS production by nanoparticles.[30,31] Possibly, a significant amount of ROS or free radicals might have been generated at 80 μg/mL concentration of LFMCSM which signifies that the primary mechanism of LFMCSM induced toxicity is due to oxidative stress, resulting in damage to cellular membranes and biological macromolecules, as reported earlier.[32,33] Our results have also demonstrated that

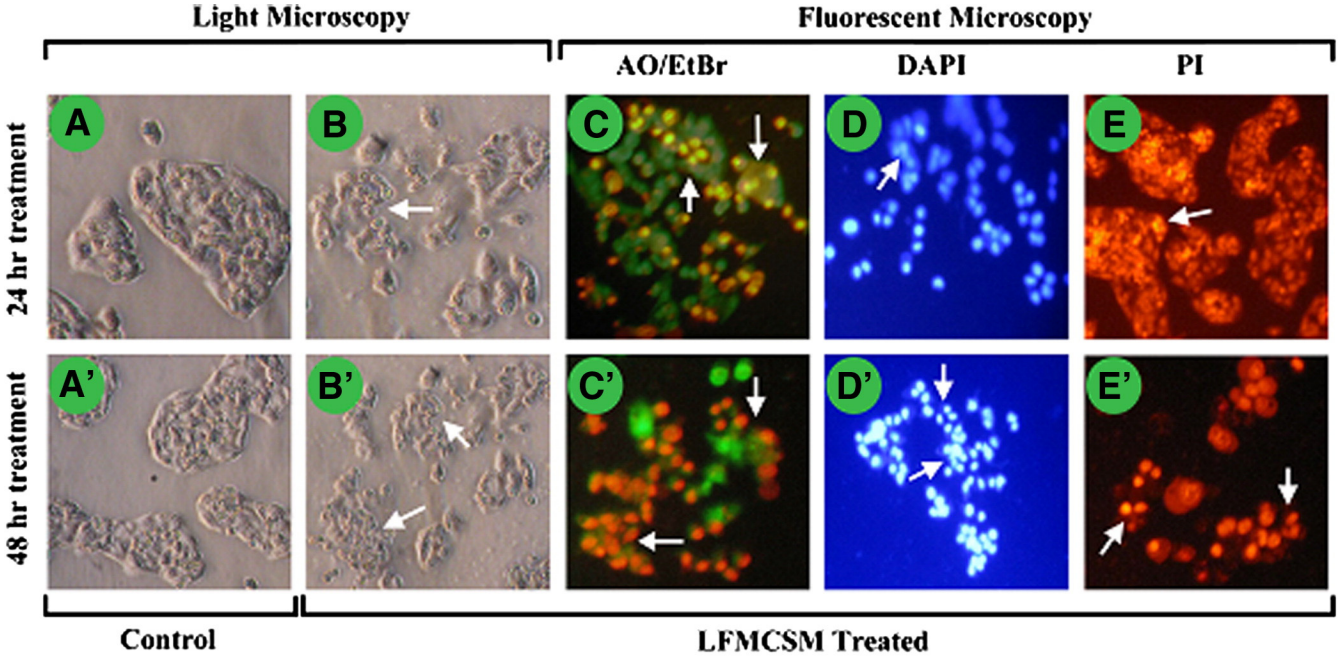

Figure 6. Light and fluorescent microscopy of HepG2 cells LFMCSM treated after 24 h **(A-E)** and 48 h **(A′-E′)**. Cell colonies are intact in untreated controls **(A** and **A′)**. Disturbance in colonies structure is evident from light microscopy **(**arrows in **B** and **B′)**. Early and late apoptotic cells are visible through AO/EtBr fluorescent staining **(C** and **C′)**. Nuclear fragmentation and blebing can be observed **(**arrows in **D** and **D′)**. Fragmentation of nuclei and micronucleus is visible **(**arrows in **E** and **E′)**.

the LFMCSMs induce DNA damage at a critical concentration of 20 μg/mL. The data suggest that the LFMCSM at lower concentrations up to 10 μg/mL might modulate the antioxidant enzymes levels, whereas, at higher concentrations, the cellular DNA repair machinery may be adversely affected, as the DNA repair genes are expressed lowly (Figure 4). It signifies that the TUNEL assay results are in accord with the MTT assay results that suggest the cytotoxic behavior of the synthesized core-shell microspheres.

On the other hand, mRNA expression study indicated the low expression of DNA repair genes (*p53*) and over expression of genes involved in DNA damage (*Caspase*-3, and *Caspase-9*) in cells at higher LFMCSM concentrations (Figure 5). It is known that the cellular DNA repair mechanisms are highly conserved,[34] and extensive DNA damage may lead to cell-cycle arrest and cell death.[35,36] Most likely, the DNA damage induced with LFMCSM at lower concentrations or below to 10 μg/mL could be adequately repaired during the G2/M phase, as no or little DNA damage (TUNEL) was also observed at this concentration. However, the greater DNA damage occurred at a threshold concentration of 80 μg/mL core-shell microspheres, as evident with the appearance of a prominent TUNEL tail due to irreparable double strand breaks. It has been reported that the LFMCSM could directly bind to DNA or repair enzymes leading to the generation of strand breaks.[37,38] Most likely, the LFMCSM induced −OH radicals are responsible for the DNA damage in the exposed cells.[39] There are contradicting results in the literature on exposure with different nanoparticles at different stages of embryo development and also with the differences in experimental models.[40] Thus, the extent of induced genetic damage, and risk assessment of the nanomaterials and nanoproducts should be assessed prior to their larger applications in spite of their apparent extraordinary advantages.

Cellular uptake

In order to investigate the biolabeling potentiality of LFMCSM in cell imaging tests, HepG2 cells were incubated with LFMCSMs for measuring the morphological changes of cells and nuclei up to 24 and 48 h by fluorescence microscopy. Fluorescence from the LFMCSMs was observed by the cells and the LFMCSMs were mainly located at the cytoplasmic regions. Fluorescence microscopy analysis was performed to confirm the cellular uptake process by the fluorescence intensities of LFMCSM in cells. In this study, fluorescence microscopy images and phase images of cells were collected through the use of a Carl-Zeiss (Axiovert, Jena, Germany) epifluorescence microscope using a dual band-pass filter. Differential interference contrast microscopy pictures of HepG2 cells (Figure 6, *A-E*) clearly show a significant difference in contrast between the untreated control cells (Figure 6, *A*) and treated cells with LFMCSM (Figure 6, *B-E*) at constant concentration. The control cells incubated without the LFMCSM showed no fluorescence under similar imaging parameters and conditions (Figure 6, *A* & *A′*) and no signs of cell damage in untreated control. However, after treatment with LFMCSM for 24 and 48 h cells are fragmented that are evident in bright field optical microscopic images as seen in Figure 6, *B* and *B′*. Further, we performed different fluorescent dyes such as Acridine orange/ethidium bromide (AO/EtBr), 4′,6-diamidino-2-phenylindole (DAPI) and propedium iodied (PI) for counter staining the HepG2 cells. These fluorescent dyes are well known to make complex with

double-stranded DNA. The first fluorescence micrographs in each series (Figure 6, *C-E*) showed the presence of healthy, round nuclei colonies like structures due to complex formation between the terminal groups of DNA and dyes which are stained green and red to yellow by AO/EtBr, blue by DAPI and red by PI, respectively (data not shown). These colonies are fragmented after co-labeling with the LFMCSM. It may be due to the existence of a large amount ROS on the surface of microspheres. These existing ROS on the surface of LFMCSM are responsible for cell apoptosis or inhibition of complex formation with cell nuclei. These observed consequences were in accord with the MTT assay, Ladder assay, TUNEL assay and qPCR results. These observed results suggest that the LFMCSM is not a suitable material for cell imaging, tracking and targeting. Further detailed study of cellular uptake mechanism was not examined here. Unfortunately, we are unable to distinguish the huge fluorescence intensity difference between untreated control cells and LFMCSM-treated cells, when we collected the emission spectra in red region. Therefore, we have collected the emission spectra for LFMCSM loaded cells in the red emission region (615 nm long pass filter). However, the confocal experiments for the best fluorescence images are currently under detailed investigations in our laboratory.

In summary, a covalent binding-copolymerization method has been established for the first time to prepare highly uniform LFMCSMs via a simple one-pot chemical route that can be used as a fluorescence probe for biomedical applications. It is proposed that Eu^{3+} cations in the solution first bind through the covalent bond with the silica (Si-O) network on the surface of mesoporous silica nanospheres to form the mesoporous shell of $Eu(OH)_3$ outside the silica core. The mesoporous features of obtained microspheres were demonstrated by TEM observation and further confirmed by small angle and wide angle X-ray diffraction pattern which showed well-defined mesoporous pores. We have shown that core-shell microsphere produces significant cytotoxicity to HepG2 cells in a dose-dependent fashion. Overall, our data suggest that LFMCSM nanoparticles may induce cell death in HepG2 cells via regulating p53, and caspase pathways. Our results suggested that particle surface properties determined by chemical composition possibly played a critical role in the programmed cell death, which is currently the best-developed paradigm for LFMCSM toxicity. Thus, the *in vitro* study showed the induction of cell death by nanoparticles demands further investigation to determine if *in vivo* challenge consequences may exist for nanoparticles application. This new method established for surface modification and bioconjugation of the microspheres would be also useful for the preparation of microspheres conjugates with other biomolecules, such as antibodies, antigens and enzymes. The present process can be extended to prepare various other luminescent functionalized mesoporous core-shell nanospheres with homogeneous morphology in terms of size, coating, increase emission properties, photostability, solubility, biocompatible and cytotoxicity, which could be usable for optical imaging of variety of biomolecules in biological and biomedical studies to ensure patient safety for potential medical applications.

Acknowledgment

Authors are thankful to Dr. V. S. Periasamy for the kind suggestions during fluorescent staining studies.

Appendix A. Supplementary data

Supplementary data to this article can be found online at http://dx.doi.org/10.1016/j.nano.2013.05.006.

References

1. Slowing II, Trewyn BG, Giri S, Lin VSY. Mesoporous silica nanoparticles for drug delivery and biosensing applications. *Adv Funct Mater* 2007;**17**:1225-36.
2. Zhao Y, Trewyn BG, Slowing II, Lin VSY. Mesoporous silica nanoparticle-based double drug delivery system for glucose-responsive controlled release of insulin and cyclic AMP. *J Am Chem Soc* 2009;**131**:8398-400.
3. Di W, Ren X, Zhao H, Shirahata N, Sakka Y, Qin W. Single-phased luminescent mesoporous nanoparticles for simultaneous cell imaging and anticancer drug delivery. *Biomaterials* 2011;**32**:7226-33.
4. Yang P, Quan Z, Lu L, Huang S, Lin J. Luminescence functionalization of mesoporous silica with different morphologies and applications as drug delivery systems. *Biomaterials* 2008;**29**:692-702.
5. Yu M, Lin J, Fang J. Silica spheres coated with YVO_4:Eu^{3+} layers via sol–gel process: a simple method to obtain spherical core-shell phosphors. *Chem Mater* 2005;**17**:1783-91.
6. Ansari AA, Labis JP. One-pot synthesis and photoluminescence properties of luminescent functionalized mesoporous SiO_2@$Tb(OH)_3$ core-shell nanospheres. *J Mater Chem* 2012;**22**:16649-56.
7. Selvan ST, Patra PK, Ang CY, Ying JY. Synthesis of silica-coated semiconductor and magnetic quantum dots and their use in the imaging of live cells. *Angew Chem Int Ed* 2007;**46**:2448-52.
8. Kim JH, Kim JS, Choi H, Lee SM, Jun BH, Yu KN, et al. Nanoparticle probes with surface enhanced Raman spectroscopic tags for cellular cancer targeting. *Anal Chem* 2006;**78**:6967-73.
9. Poovarodom S, Bass JD, Hwang SJ, Katz A. Investigation of the core-shell interface in gold@silica nanoparticles: a silica imprinting approach. *Langmuir* 2005;**21**:12348-56.
10. Santra S, Zhang P, Wang K, Tapec R, Tan W. Conjugation of biomolecules with luminophore-doped silica nanoparticles for photostable biomarkers. *Anal Chem* 2001;**73**:4988-93.
11. Tang F, Li L, Chen D. Mesoporous silica nanoparticles: synthesis, biocompatibility and drug delivery. *Adv Mater* 2012;**24**:1504-34.
12. Santra S, Tapec R, Theodoropoulou N, Dobson J, Hebard A, Tan W. Synthesis and characterization of silica-coated iron oxide nanoparticles in microemulsion: the effect of nonionic surfactants. *Langmuir* 2001;**17**:2900-6.
13. Richardson FS. Terbium(III) and europium(III) ions as luminescent probes and stains for biomolecular systems. *Chem Rev* 1982;**82**:541-52.
14. Ansari AA, Alam M, Labis JP, Alrokayan SA, Shafi G, Hasan TN, et al. Luminescent mesoporous $LaVO_4$:Eu^{3+}core-shell nanoparticles: synthesis, characterization, biocompatibility and their cytotoxicity. *J Mater Chem* 2011;**21**:19310-6.
15. Parchur AK, Ningthoujam RS. Preparation and structure refinement of Eu^{3+} doped $CaMoO_4$ nanoparticles. *Dalton Trans* 2011;**40**:7590-4.
16. Judd BR. Optical absorption intensities of rare-earth ions. *Phys Rev* 1962;**127**:750-61.
Ofelt GS. Intensities of crystal spectra of rare-earth ions. *J Chem Phys* 1962;**37**:511-611.
17. Hussain SM, Hess KL, Gearhart JM, Geiss KT, Schlager JJ. In vitro toxicity of nanoparticles in BRL 3A rat liver cells. *Toxicol In Vitro* 2005;**19**:975-83.

18. Fubini B, Hubbard A. Reactive oxygen species (ROS) and reactive nitrogen species (RNS) generation by silica in inflammation and fibrosis. *Free Radic Biol Med* 2003;**34**:1507-16.
19. Wang JJ, Sanderson BJS, Wang H. Cytotoxicity and genotoxicity of ultrafine crystalline SiO_2 particulate in cultured human lymphoblastoid cells. *Environ Mol Mutagen* 2007;**48**:151-7.
20. Fenoglio I, Croce A, Renzo FD, Tiozzo R, Fubini B. Pure-silica zeolites (porosils) as model solids for the evaluation of the physicochemical features determining silica toxicity to macrophages. *Chem Res Toxicol* 2000;**13**:489-500.
21. Stadtman ER. Oxidation of free amino acids and amino acid residues in proteins by radiolysis and by metal-catalyzed reactions. *Annu Rev Biochem* 1993;**62**:797-821.
22. Thrall L. Exposure of engineered nanoparticles to human lung epithelial cells: influence of chemical composition and catalytic activity on oxidative stress. *Environ Sci Technol* 2007;**41**:3791-2.
23. Wu S, Ko YS, Teng MS, Ko YL, Hsu LA, Hsueh C, et al. Adriamycin-induced cardiomyocyte and endothelial cell apoptosis: in vitro and in vivo studies. *J Mol Cell Cardiol* 2002;**34**:1595-607.
24. Chen JP, Patil S, Seal S, McGinnis JF. Rare earth nanoparticles prevent retinal degeneration induced by intracellular peroxides. *Nature Nanotechnol* 2006;**1**:142-50.
25. Patra CR, Bhattacharya R, Patra S, Basu S, Mukherjee P, Mukhopadhyay D. Lanthanide phosphate nanorods as inorganic fluorescent labels in cell biology research. *Clin Chem* 2007;**53**:2029-31.
26. Patra CR, Bhattacharya R, Patra S, Vlahakis NE, Gabashvili A, Koltypin Y, et al. Pro-angiogenic properties of europium(III) hydroxide nanorods. *Adv Mater* 2008;**20**:753-6.
27. Bhakta G, Sharma RK, Gupta N, Cool S, Nurcombe V, Maitra A. Multifunctional silica nanoparticles with potentials of imaging and gene delivery. *Nanomedicine* 2011;**7**:472-9.
28. Xu A, Chai Y, Nohmi T, Hei TK. Genotoxic responses to titanium dioxide nanoparticles and fullerene in gpt delta transgenic MEF cells. *Particle and Fibre Toxicology* 2009;**6**:3.
29. Pasqua AJD, Sharma KK, Shi YL, Toms BB, Ouellette W, Dabrowiak JC, et al. Cytotoxicity of mesoporous silica nanomaterials. *J Inorg Biochem* 2008;**102**:1416-23.
30. Stone V, Shaw J, Brown DM, MacNee W, Faux SP, Donaldson K. The role of oxidative stress in the prolonged inhibitory effect of ultrafine carbon black on epithelial cell function. *Toxicol In Vitro* 1998;**12**: 649-59.
31. Oberdorster G, Oberdorster E, Oberdorster J. Nanotoxicology: an emerging discipline evolving from studies of ultrafine particles. *Environ Health Perspect* 2005;**113**:823-39.
32. Nel A, Xia T, Madler L, Li N. Toxic potential of materials at the nano level. *Science* 2006;**311**:622-7.
33. Shukla RK, Sharma V, Pandey AK, Singh S, Sultana S, Dhawan A. ROS mediated genotoxicity induced by titanium dioxide nanoparticles in human epidermal cells. *Toxicol In Vitro* 2011;**25**:231-41.
34. Ferreira CG, Epping M, Kruyt FA, Giaccone G. Apoptosis: target of cancer therapy. *Clinic Cancer Res* 2002;**8**:2024-34.
35. Konopa J. G2 block induced by DNA cross linking agents and its possible consequence. *Biochem Pharmacol* 1988;**37**:2303-9.
36. Tsao YP, D'Arpa P, Liu LF. The involvement of active DNA synthesis in camptothecin-induced G2 arrest: altered regulation of p34cdc2/cyclin B. *Cancer Res* 1992;**52**:1823-9.
37. Hartwig A. Carcinogenicity of metal compounds: possible role of DNA repair inhibition. *Toxicol Lett* 1998;**102–103**:239-355.
38. Reeves JF, Davies SJ, Dodd NJF, Jha AN. Hydroxyl radicals (−OH) are associated with titanium dioxide (TiO_2) nanoparticle-induced cytotoxicity and oxidative DNA damage in fish cells. *Mutat Res* 2008;**640**: 113-22.
39. Challier JC, Panigel M, Meyer E. Uptake of colloidal 198Au by fetal liver in rat, after direct intrafetal administration. *Int J Nucl Med Biol* 1973;**1**:103-6.
40. Bosman SJ, Nieto SP, Patton WC, Jacobson JD, Corselli JU, Chan PJ. Development of mammalian embryos exposed to mixed-size nanoparticles. *Clin Exp Obstet Gynecol* 2005;**32**:222-4.